THE JOURNAL OF PHYSICAL CHEMISTRY B

 VOLUME 105, NUMBER 5, FEBRUARY 8, 2001

FEATURE ARTICLE

# Molecular Dynamics Study of Bacteriorhodopsin and the Purple Membrane

**Jérôme Baudry,[†] Emad Tajkhorshid,[†] Ferenc Molnar,[†] James Phillips,[†,‡] and Klaus Schulten*,[†,‡]**

*Beckman Institute and Department of Physics, University of Illinois at Urbana−Champaign, Urbana, Illinois 61801*

*Received: March 7, 2000; In Final Form: October 25, 2000*

Vectorial proton translocation through membranes is a fundamental energy conversion process in biological cells. Bacteriorhodopsin (bR) is a membrane protein that acts as a light-driven, voltage-sensitive proton pump in the purple membrane (PM) of *Halobacterium salinarum* and achieves its biological function by cycling through a reaction sequence that includes ultrafast (∼500 fs) events, intermediate ($\mu$s) as well as slow (∼10 ms) steps. bR is of utmost simplicity in comparison with other proton translocating bioenergetic proteins and, therefore, constitutes an ideal model for the study of this process. The PM involves a highly structured supramolecular organization and is fundamental for the in vivo functioning of bR. Over the last 10 years, crystal structures of bR have become available at increasing resolution. The most recent structures resolve many of the lipids of the PM and provide atomic level detail of bR at below 2 Å resolution. Fundamental for an understanding of the function of bR is internal water that participates in proton pumping. Several water molecules have been resolved now crystallographically in two channels, on the extracellular and on the intracellular side of bR. We show that free energy perturbation theory can place water molecules in bR, with results that compare well with the observed water molecules, and we apply the method to predict water movement during bR's photocycle. A preliminary simulation illustrates that water molecules may indeed be displaced during the photocycle, after retinal undergoes an *all-trans* → 13-*cis* isomerization, and that this displacement may constitute a mechanism for proton pumping. A key advance reported in this feature article is the integration of the available bR structures into a model for the entire PM. This hexagonally periodic, lamellar model has been hydrated and refined through a constant pressure molecular dynamics simulation. The resulting structure connects extracellular bulk water with water molecules and key side groups in the interior of bR, permitting a seamless overall description of the proton path in the PM, from intracellular to extracellular space. For the first time, a complex cellular reaction can be accounted for in full atomic detail in its complete native environment.

## Introduction

Living cells have learned during evolution to use physical and chemical properties of macromolecules and their assemblies for their benefit. Physical chemists naturally would like to know what cells have learned that is not yet found in textbooks, but many shy away from studies of in vivo cellular systems since such systems are insufficiently characterized, leaving wide knowledge gaps in regard to exact composition, structure, and function. Most researchers remained focused instead on small

[†] Beckman Institute.
[‡] Department of Physics.

10.1021/jp000898e CCC: $20.00 
Published on Web 01/10/2001

and purified in vitro systems at the price of nagging doubts that such idealized systems might not permit true understanding of the integration of molecular building blocks into cellular functions.

Science develops in leaps and what seemed unachievable one day often becomes possible the next. This Feature Article wants to introduce one such instance in which a complete cellular function, use of sunlight to generate a proton-based potential gradient across a cellular membrane, can be studied today for an entire cellular apparatus in which essentially every participating atom is known, leaving no room for speculation in regard to composition, structure, and function. This apparatus poses a great challenge to physical chemists: can one explain the functioning of this system at the same level of rigor that we have come to accept for smaller in vitro systems.

The cellular apparatus that recently revealed itself in full detail is the purple membrane (PM) of certain salt loving archaebacteria, e.g., of *Halobacterium salinarum.* It has been known since a long time that the cellular membrane of this bacterium contains patches of purple colored two-dimensional crystalline aggregates of proteins and lipids, the PM. This membrane converts sunlight into a potential difference between the interior and the exterior of the bacterial cell by pumping protons out of the cell. The PM contains multiple copies of a single protein, called bacteriorhodopsin (bR), named so because of its close homology to rhodopsin, the protein that is the light receptor of animal vision. bR had been investigated in its monomeric form under in vitro conditions, studies which experienced a great boost once the structure of the individual protein had become available. In addition to bR, PM contains 10 haloarcheal lipids per protein unit that have identical saturated side chains, but differ in the nature of their polar heads.

**Bacteriorhodopsin.** bR is a 26 kDa transmembrane protein that acts as the light-driven proton pump in the PM. The protein contains seven α-helices that enclose an *all-trans*-retinal chromophore linked via a protonated Schiff base to residue Lys216. Upon light absorption, retinal undergoes an isomerization process that results under normal conditions in the translocation of a proton from the cytoplasmic side to the extracellular side of the membrane (quantum yield ∼0.67[1,2]). For reviews, see refs 3 and 4 as well as the summary of theoretical work in ref 5. The dynamics of the excited state of the retinal in bR and the effect of the protein environment on the rate of its photoisomerization have been experimentally investigated.[2,6−8] The dynamics of *all-trans*- and 13-*cis*-retinal Schiff base have also been recently studied in different solvents by means of picosecond transient spectroscopy.[9]

Vectorial proton translocation through membranes is a fundamental energy conversion process in biological cells. bR's utmost simplicity in comparison with other proton translocating bioenergetic proteins makes it an ideal model for the study of this process. The intrinsic properties of bR have also been used in technological applications, such as new molecular electronic devices based on bR's optical properties.[10,11]

A remarkable aspect of bR is that the most essential aspects of its functioning are still subject of intense work and controversy, despite decades of research and impressive breakthroughs. Why should one then want to answer today the question of how bR converts light energy into a proton gradient? There is great reason for optimism now since we have finally available high-resolution structures of bR and even of some of its photocycle intermediates on which the required physical analysis can be based. Over the last 10 years, crystal structures of bR with ground-state *all-trans*-retinal have become available at increasing resolution.[12−25] These structures, together with the experimental data collected on bR's function, provide insight into the proton pathway in bR, but not into the pump mechanism; i.e., they do not explain how free energy stored in the initial photoproduct is funneled into proton translocation and thermal reisomerization under control of the membrane voltage. Knowing where protons are conducted does not imply knowing why protons are conducted! Recent structures of different intermediates of bR[21−23,25] are of great value. Although they may not reveal the dynamics of the pump mechanism, they provide stationary, guiding points for conducting and verification of molecular dynamics simulations.

There exist great incentives for theoretical and computational studies of bR. Proton translocation is a dynamic process and an explanation of bR's proton pumping will require an extrapolation from the available static structure of bR in its ground state as well as an interpolation between structurally observed pump cycle intermediates, both of which can be achieved through modeling. Furthermore, proton translocation likely involves only very minute motions partially below the resolution of observation, but accessible to molecular modeling. This had been argued in refs 5 and 26−29. These studies stressed that internal water molecules are likely key players in proton pumping.

Major progress in identifying internal and some external water molecules was achieved by the recent crystallographic studies of bR.[16,17,19−22] Free energy perturbation theory has been used to calculate the probability of occupation of various sites by water molecules in the retinal binding region.[30,31] In addition, there is also spectroscopic information that bears on the vibrational modes and location of the water molecules.[32−35] Force fields for water−water and water−amino acid interactions that are presently developed to achieve agreement with spectroscopic data promise greatly improved descriptions of proton pumping in bR.

**Purple Membrane.** Methodological advances permit modelers today to simulate integral membrane systems like the entire PM, as well as to provide highly accurate quantum chemical descriptions of potential energy surfaces for multiple (ground and excited) states, both preconditions for an explanation of bR's pump mechanism.[36] The PM involves a highly structured supramolecular organization, and is fundamental for the in vivo functioning of bR. The significance of lipid molecules in the function of bR has been experimentally demonstrated.[37] Variations in hydration levels of the PM were shown to be correlated with the functioning of bR,[38−42] specifically with the conformational flexibility of the protein.

bR had been simulated previously in a lipid patch as reported in ref 43. This study stressed the critical role of lipids and hydration on the dynamics of bR, but the quality of the protein−lipid bilayer model did not permit an investigation of structural details, e.g., of the connection between internal and external water molecules or of the influence of the lipid matrix on bR dynamics. Such investigation requires an accurate model of the integrated supramolecular systems forming the PM. The prerequisite model can be provided through computational techniques that integrate and complement the structural data available today.

In this paper, we present a model of the PM that has been constructed accordingly by means of molecular dynamics simulations. The goal of the present paper is to present state of the art modeling techniques that can be applied to bR and PM simulations. We present a model of the PM and discuss the possible applications of such a model.

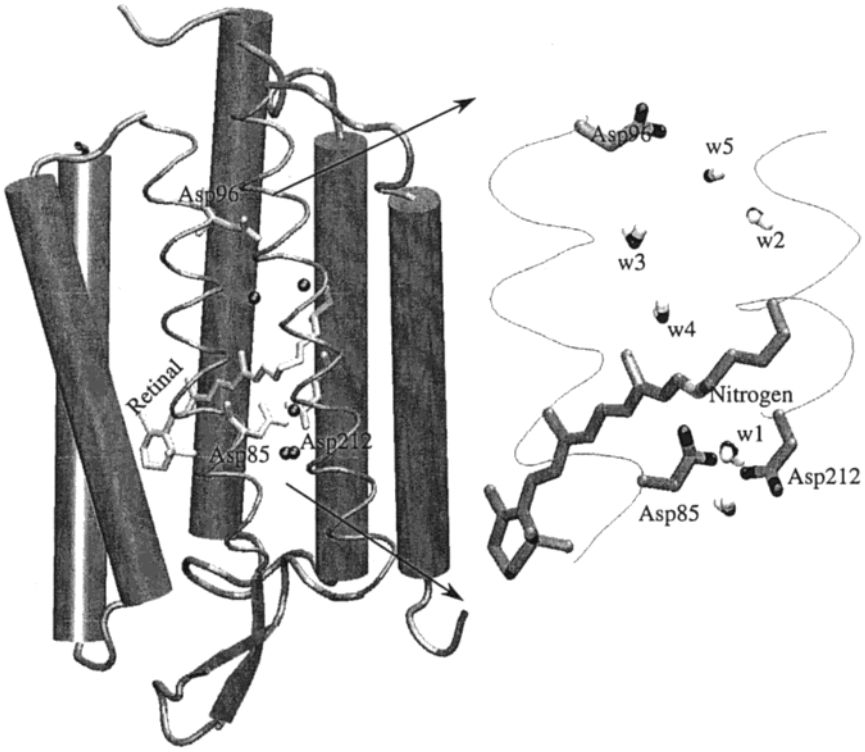


**Figure 1.** (Left) bR monomer. Helices are drawn as cylinders, $\beta$-sheets as arrows. Retinal, Asp85, Asp212, and Asp96 are drawn in stick representation; internal water molecules in the retinal binding site are drawn as black spheres. (Right) retinal binding site, equilibrated at 300 K from the structures reported in refs 16 and 17 (see text). Water molecules labeled W1 to W5 (see text) were found to have a significant probability of existence.

The necessary computations are methodologically challenging, both due to problems in describing faithfully lamellar membranes at constant pressure with full electrostatic interactions, and due to the large size of the unit cell of the hydrated PM. Below we describe the necessary computations along with simulations of single bR dynamics that motivate the work on the entire PM. We outline the simulation methods used and describe in detail how, from the available crystallographic structures, a model of the PM was obtained. We demonstrate then that free energy perturbation theory today can place internal water in bR accurately. We exploit this capability to show that the photoisomerization of retinal in bR is likely to induce a structurally significant reordering of internal water molecules. We describe then the properties of the PM model constructed, outline the simulations that equilibrated the model, and report on one key attribute of the model, namely, the arrangement of external water.

## Methods

Simulations were carried out for single bR and the PM. Methods employed on single bR were those described in ref 31; the methods used for simulating the PM are described further below.

**Placement of Internal Water Molecules.** Among the recent crystal structures of bR, four structures[16,17,19,20] propose positions for internal water molecules located in the protein. After initial controversy, recent structures of bR[19,20] have converged in most respects, in particular, in regard to the locations of most of the internal water molecules. However, water molecule W2 (see Figure 1), which is present in ref 20, has not been reported in refs 17 and 19. This disagreement exemplifies why computational placement of water molecules is of importance, even though structures of bR continue to improve. There exist further reasons for computational water placement: because of high thermal mobility, water molecules may not be crystallographically discernible; and water molecules are likely to rearrange during the pump cycle and might not be fully resolved in the structures of the intermediates; lastly, water molecules are likely to enter bR during the photocycle (M state) and their number and location may be subject to hysteresis that might be difficult to observe crystallographically.

The impressive power of computational placement of water molecules in a protein had been demonstrated in earlier work on cytochrome *c* oxidase.[44] This work successfully predicted many features of proton channels and water distribution in this system, which were only later revealed in resolved structures, e.g., in ref 45. In comparison with the work in ref 44, our present approach to water placement has been improved in that we determine now the thermodynamic stability of water molecules using free energy perturbation theory following the protocol of Roux et al.[30] The method permits calculation of the free energy cost of transferring a water molecule from bulk water to a possible hydration site in the protein, and assessment of the associated probability of occupancy of the given hydration site.

The stability of water molecules was predicted at the various positions suggested by the crystal structures using a monomeric bR model. The bR structure reported in ref 16 (PDB entry 1AP9) was used as the initial structure. In a successive structure with improved resolution,[17] the placement of a water molecule between the Schiff base, Asp212, and Asp85, and reorientation of Asp212 to establish a hydrogen bond with Tyr185, are in agreement with spectroscopic data.[46] Water molecules in the cytoplasmic part of the proton channel were placed following ref 16, i.e., a water molecule hydrogen-bonded to Asp96, a water molecule close to atom $C_{20}$ of retinal and hydrogen-bonded with the hydrogen of atom $C_{15}$, a water molecule hydrogen-bonded with the carboxyl group of Lys216, and a fourth water molecule hydrogen-bonded to Trp182.

A cycle of minimizations and MD simulations was performed, using the program CHARMM[47] with harmonic constraints on

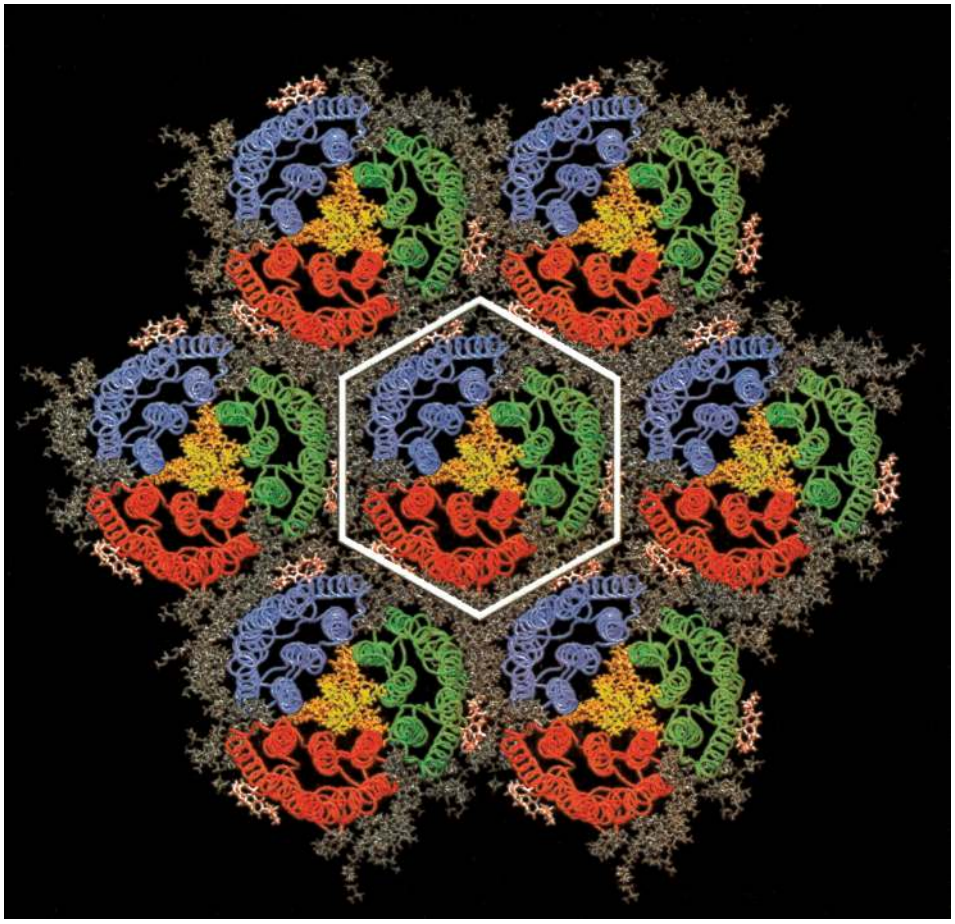

**Figure 2.** Top view of a purple membrane patch that includes 21 bacteriorhodopsins in seven adjacent unit cells. The hexagonal unit cell is shown in the middle of the patch; its boundary is indicated by white lines. For the color code see Figure 3. All figures in this article were produced with the program VMD.[61]

bR's atoms progressively released,[30,31] with a total simulation time of 75 ps. This equilibration procedure was found to lead to a bR structure that was stable over a period of 500 ps.[48,49] The equilibrated structure and its stable water molecules are presented in Figure 1. The average position of the water molecules located in the retinal binding site, and the rms of their fluctuations were also calculated. The geometry of retinal in the binding pocket and the water/retinal interactions have been analyzed[31] for the resulting average structure as well as for an average structure of an MD run starting from the structure reported in ref 17. Despite differences in the initial atomic positions, MD simulations resulted in a convergence of the equilibrated structures at room temperature[31] within their rms values. The new structures, i.e., those in refs 19 and 20, are so close that within MD descriptions differences are irrelevant.

The free energy of transfer of a water molecule into the protein is calculated using a so-called alchemical reaction, in which a water molecule is annihilated in several steps during the course of the simulation. The protocol has been described elsewhere[30] and is followed in the present calculations. The free energy perturbation calculations were run for five water molecules in the retinal binding site, presented in Figure 1. Each of these simulations lasted 50 ps. The program CHARMM[47] was used for this purpose.

**Construction and Equilibration of PM Model.** The PM model was built by constructing a hexagonal unit cell, and replicating it in space using periodic boundary conditions. The unit cell contains three monomeric bR molecules, 28 lipid molecules, and 2804 water molecules, altogether 23 783 atoms. Figure 2 shows a top view of the modeled PM patch including the central unit cell and the surrounding six image cells. Figures 3, 4, and 5 show different views of the modeled unit cell. The information obtained from several crystal structures of bR was used to assemble all the parts of the unit cell.

*Crystal Structures Used*. Four structures were used for building the unit cell: (i) the bR trimer structure published by Essen et al.[18] (structure 1, PDB entry 1BRR); (ii) a monomeric bR structure (structure 2, PDB entry 1QHJ) obtained by Pebay-Peyroula et al.;[19] (iii) a monomeric bR structure (structure 3, PDB entry 1C3W) obtained by Luecke 11 et al.;[20] (iv) a monomeric bR structure obtained by Grigorieff et al. (structure 4, PDB entry 2BRD).[13]

Structure 1 (S1)[18] has 2.9 Å resolution and was obtained from a monoclinic crystal form of bR. This structure contains atomic coordinates for three bR monomers (labeled A, B, and C) forming a trimer similar to bR in the native PM. S1 contains coordinates for residues starting from Ala3 in monomer A, Ala2 in monomer B, and Alal in monomer C to Ala232 in all monomers. S1 also contains a number of lipid molecules associated with the protein: seven out of the 30 lipids associated with the bR trimer were structurally resolved in S1. In particular, three glycolipids (S-TGA-1) were located in the central compartment of the bR trimer, and two of them were observed with their polar heads resolved. In addition, three lipids were observed as single phytanols in hydrophobic regions located between helices AB of a bR monomer and helices DE of the neighboring monomer.

Structure 2 (S2)[19] was obtained by X-ray diffraction using

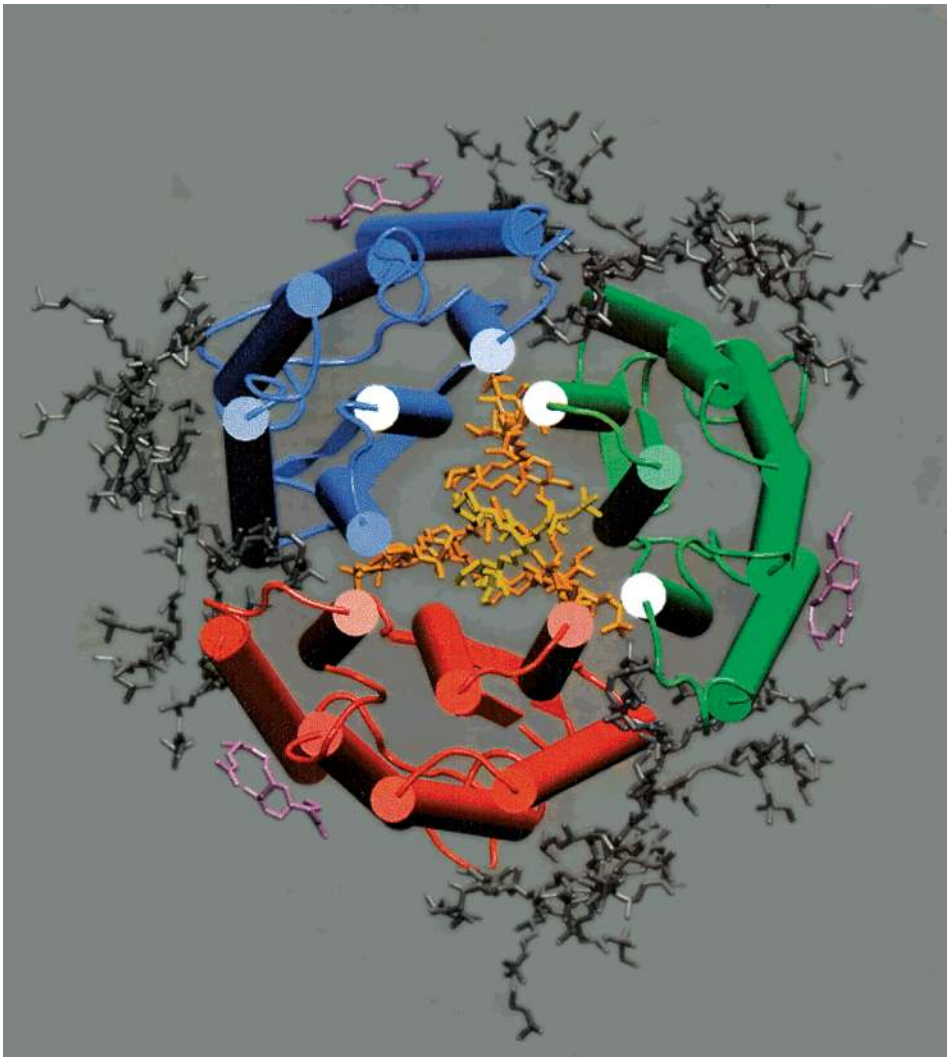

**Figure 3.** Top view of the hexagonal unit cell containing the bR trimer and lipid molecules. Extratrimer PGP molecules are shown in gray; extratrimer squalene molecules are shown in purple. Intratrimer glycolipid molecules (cytoplasmic side of the PM) are shown in orange; the intratrimer PGP molecules (intracellular side) is shown in yellow. The three bR monomers are shown in blue, red, and green cartoon representations.

hexagonal bR microcrystals, following the crystallization procedure described in ref 16. S2 is a 1.9 Å resolution structure, which is not compromised by hemihedral twinning. S2 contains the coordinates of a monomeric bR molecule starting from residue Thr5 to residue Ala232. In addition, it contains several internal water molecules: one water molecule in the space between Asp96 and retinal, four water molecules between retinal and Arg82, and nine water molecules between Arg82 and the extracellular side of the protein. Additional water molecules have been observed outside the protein, both on the cytoplasmic and extracellular sides. S2 also contains nine lipid molecules. The position of one of these lipid molecules corresponds to one of the central glycolipids (S-TGA-1) reported in S1. Another lipid (ARC506) corresponds to a phytanol. The other seven lipid molecules reported in S2 are external lipids, which are located between the bR trimers in the PM. The polar heads of these seven lipids were not resolved. The protein structure agrees closely with structure S3 introduced now.

Structure 3 (S3)[20] was obtained by X-ray diffraction using hexagonal bR microcrystals as in ref 19. S3 is a 1.55 Å resolution structure that contains coordinates for a monomeric bR from residue Thr5 to residue Gly231, with the exception of the loop connecting helices E and F, i.e., between residues Phe156 and Ser162. Several water molecules are also observed in S3: two water molecules between Asp96 and retinal, four water molecules between retinal and Arg82, and 15 other water molecules not located between Asp96 and Arg82. S3 contains the coordinates of several lipid chains, as well as one squalene molecule, which is located in a groove near helix G.

Structure 4 (S4)[13] was obtained by cryoelectron microscopy. This structure along with earlier structures from the group of Henderson were actually the first reported on bR and despite the relatively low resolution, in particular, in the loop regions, most of its features have been confirmed through the later crystallographic studies. However, S4 does not include internal water molecules and details of molecular geometries in the retinal binding site, that may be crucial for an explanation of bR's pump mechanism, and that were revised in the better resolved structures S2 and S3.

*Arrangement of the bR Trimer*. The coordinates of the bR trimer reported in S1 were used to build the protein model. S1 features different conformations for the three monomeric bRs in the trimer. These structural differences between the three monomeric bR molecules in S1, accordingly, lead us to a bR trimer with a structural diversity, which could not be obtained if we had used monomer structures from S2 or S3 and had generated the bR trimer assuming a 3-fold symmetry. Since S1 does not contain coordinates for the entire sequences of bR in the three monomeric units, the proteins had to be completed

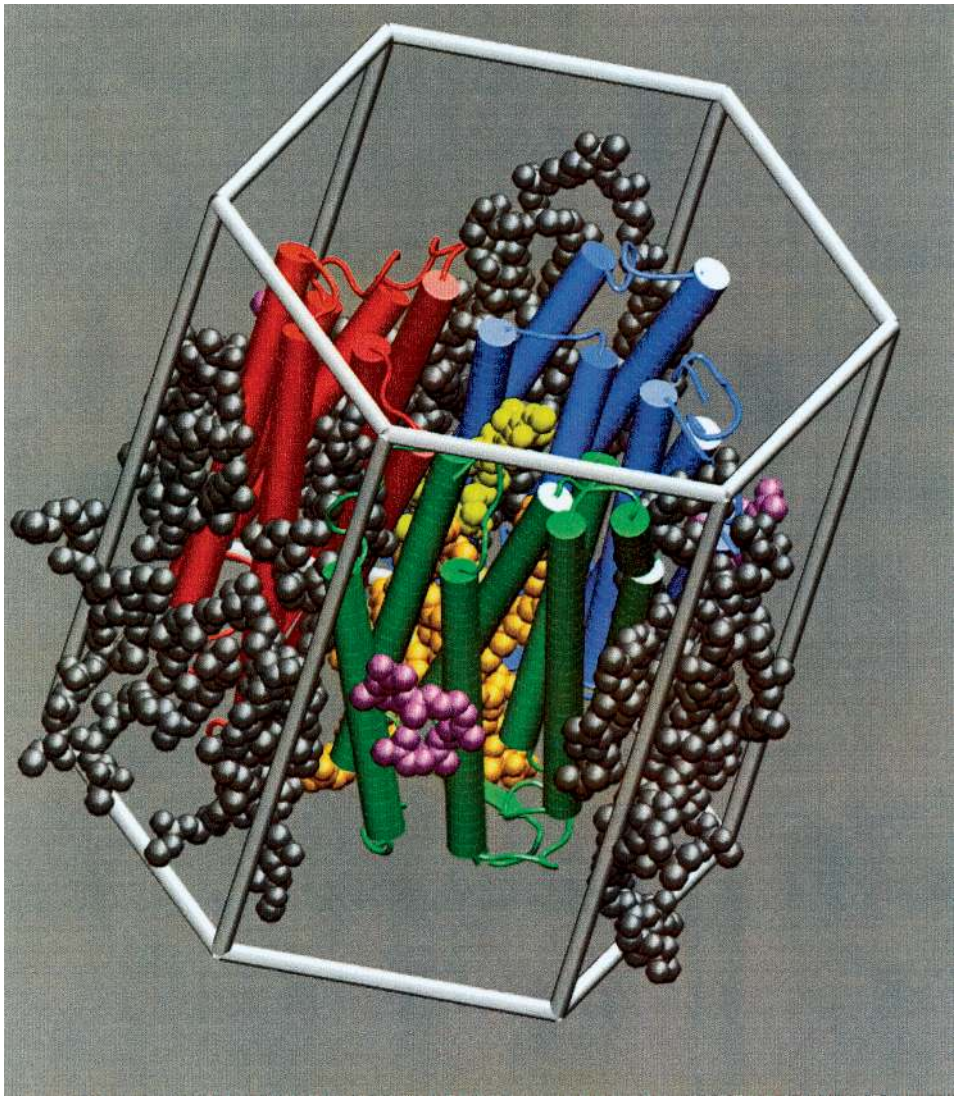

**Figure 4.** Side view of the hexagonal unit cell. The edges of the unit cell are indicated by white lines. Same color code as Figure 3.

through modeling. This was achieved as follows. Monomer B in S1 does not contain the coordinates of the Arg227 side chain. The chain was added using Quanta98 (Molecular Simulations Inc.). Missing side chain atoms for residues 225, 227, 229, and 230 in monomer A, and for residues 227, 229, and 230 in monomer C were added to the model according to the conformation of these side chains in monomer B. The missing residues near the N-terminal regions of the monomers were added by Quanta98, assuming the same dihedral angle ($\phi$, $\psi$, $\chi$) values as assumed for monomer B.

Monomers A, B, and C reported in ref 18 differ also in the C-terminal region in regard to their amino acid composition: different side groups are Ala3 and Ile4 in A, Ala3 and Ala4 in B, and Gln3 and Ile4 in C. The composition of C is the native one and, accordingly, we mutated the respective side groups in A and B, using for the replacement side group geometries as observed for C. Hydrogen atoms were added to the resulting bR trimer employing the H-build command of CHARMM within Quanta98. Apart from Asp96 and Asp115, which were protonated, default protonation states were assumed for all residues.

*Arrangement of Lipids in the Unit Cell.* bR trimers are organized in the PM in a two-dimensional hexagonal lattice. The two-dimensional crystalline state is important for the in vivo physiology of bR.[50] The protein/lipid ratio in the PM is exceptionally high and, except for squalene residues, the lipids all have the same saturated, branched-alkyl side chains, and differ only in their polar heads: phosphatidylglycerol, phosphatidylglycerol methyl ester, and a sulfated triglycoside lipid. The number of lipid molecules per bR monomer in the PM is about 10.

The glycolipids are crucial for the stability of the PM[51] and partition exclusively on the extracellular leaflet of the cell membrane.[52] A recent study on detergent-treated PMs has shown that full restoration of the normal photocycle behavior can be achieved by incubating the damaged membranes with a combination of squalene and phosphatidyl glycerophosphate lipids.[37] Although the experimental conditions used in that study did not disrupt the trimer structure of bR, major disruptions in the photocycle of the detergent-treated PM were observed.[37] These authors reported also that full restoration of the PM from detergent-treated membranes requires squalene molecules and that their removal from the PM leads to modified photocycle kinetics.

In the PM model constructed, all of the lipids are in the form of phosphatidyl glycerol phosphate (PGP), except for glycolipids and squalene molecules. Structures S1, S2, and S3 contain partial or complete atomic coordinates of these lipid molecules that suffice to build the lipid components of the PM. Table 1 lists the names, origins (which crystal structure), and locations of the lipid molecules incorporated in the PM. The lipids can be

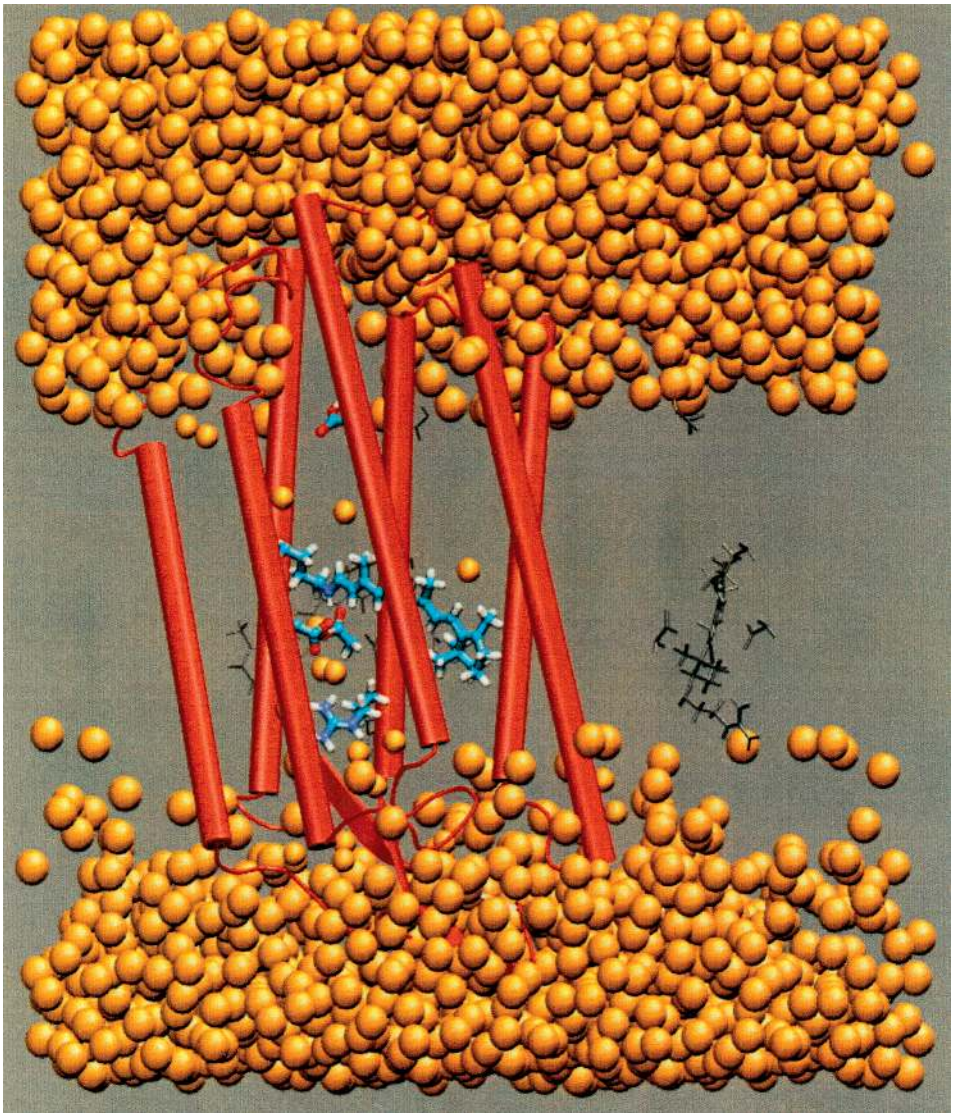

**Figure 5.** View of a bR monomer in the hydrated unit cell. The monomer is displayed in red cartoon representation, Residues Asp96, Asp212, Asp85, and Arg82 are displayed in CPK colors and in stick representation. External water molecules are shown as large orange spheres; internal water molecules are presented as small orange spheres.

**TABLE 1: List of Lipid Molecules Included in the PM Model, and of the Corresponding Molecules' Names in Structures S1−S4 (See Text). The Molecules Incorporated in the PM Model Are Indicated in Boldface**

| present model | structure S2[19] | structure S3[20] | structure S1[18] | structure S4[13] | location in bR trimer[e] | location in unit cell[f] |
|---|---|---|---|---|---|---|
| PGP-1A | **ARC 501** | LIP 601 & 612[a] | | DPG 264[a,b] | ET | EC |
| PGP-2A | **ARC 502** | LIP 602 & 603[a] | | DPG 263[b] | ET | EC |
| PGP-3A | **ARC 503** | LIP 604[a] | | DPG 262[b] | ET | EC |
| PGP-4A | **ARC 504** | LIP 611[a] | | DPG 265[b] | ET | EC |
| PGP-5A | **ARC 505** | LIP 610[a] | | DPG 267 | ET | IC |
| PGP-6A | **ARC 506** | LIP 612[a] | ARC 7[a] | DPG 269[c] | ET | IC |
| PGP-7A | **ARC 507** | LIP 609[a] | | DPG 268 | ET | IC |
| SQ-A | ARC 508[a] | **SQU 701** | OCT 5[a] | | ET | *d* |
| GLC-AC | | | *g* | | IT | EC |
| GLC-AB | | | *g* | | IT | EC |
| GLC−BC | | | *g* | | IT | EC |
| PGP−INTER | | | | | IT | IC |

[a] Partial agreement only. [b] From image (periodic boundary conditions) of monomer C's lipid molecule. [c] Lipid molecule from monomer B. [d] Squalene is close to the center of the membrane plane. [e] ET indicates extra-trimer location, IT indicates intra-trimer location. [f] EC indicates extracellular location, IC indicates cytoplasmic location. [g] **GLC AC**: GAS 36, ARC 31, MAN 35, GLC 34, ARC 32, GLZ 33; **GLC AB**: GAS 26, ARC 22, MAN 25, GLC 24, ARC 21, GLZ 23; **GLC BC**: ARC 12, ARC 11, GLZ 13.

categorized into four classes: (i) phytanol lipid molecules located outside the bR trimer, (ii) squalene, (iii) glycolipids located inside the bR trimer on the extracellular side of the membrane, and (iv) lipid molecules located inside the bR trimer on the intracellular side of the membrane. Figures 3, 4, and 5 show the structure of the hexagonal unit cell model and the location of these four classes of lipids.

Compared to the convergence of the protein structures and

internal water molecules in the recently published data,[17,19,20] the geometries reported for the lipid molecules show much less consistency between different experimental structures. The observed fatty acid chains can be combined and modeled in many different ways. We have selected a combination of the most consisitently resolved lipid molecules for our PM model. Further observations will likely lead to improvements of the suggested structure. For example, a lipid molecule (residue L2P300) reported in one of the most recent structures of bR (PDB entry 1QM8, Kouyama et al., to be published) can be well fitted into our model (not included in the present paper).

*Arrangement of PGP Lipids Outside bR Trimer*. Each monomer in the unit cell is associated with seven lipid molecules located in the exterior of the bR trimer. These lipid molecules (labeled PGP1 to PGP7 in our model) were assigned according to the lipids labeled ARC501 to ARC507 in S2. Lipids ARC506 and ARC507 in S2 are in partial agreement with lipid molecules in S3[20] and S4.[13] We chose lipids ARC501 to ARC507 in S2 for our assignment since the molecules were entirely defined structurally through atomic coordinates, except that coordinates for the polar heads were missing. These lipids were modeled as PGP by addition of the polar heads to lipids PGP1 to PGP7, using visual inspection and ensuring that no polar head had bad van der Waals contacts with surrounding atoms in the PM.

To achieve suitable positions for the PGP lipid molecules, structure S2 (containing the coordinate information of lipids) was superimposed on the bR monomers A, B, and C via a best fit of $C_\alpha$ atoms, and the coordinates of lipids ARC501 to ARC507 in structure S2 were copied then to the unit cell model containing the trimer from structure S1. After this step, each monomer in the unit cell model contains its own set of lipid molecules PGP1 to PGP7, therefore leading to 21 PGP molecules in the extratrimer zone. Nine of these PGP lipids (three per monomer) are distributed on the intracellular side of the PM (PGP5, PGP6, and PGP7); the remaining 12 PGP molecules (four per monomer) are distributed on the extracellular side (PGP1 to PGP4). The PGP lipids are depicted in Figures 3 and 4.

*Arrangement of Squalene*. The unit cell model contains three squalene molecules (one per monomer). The coordinates of squalene were taken from structure S3 (residue SQU701, see Table 1). Before using the squalene residue in S3, three missing methyl groups were added to atoms C7, C18, and C23 (numbers refer to SQU701 in S3), the valences of the carbon atoms were fixed (all of the carbon atoms were defined as $sp^3$, except for atom number 7, 9, 12, 14, 17, 18, 22, and 23, which were defined as $sp^2$), and hydrogens were added to the residue. Superposition of S3 on monomers A, B, and C in the unit cell by means of least-squares deviation between $C_\alpha$ carbons yielded the positions of squalene in the PM model. The squalene molecules are represented in purple in Figures 3 and 4.

For S2 the authors in ref 19 report an eighth lipid, ARC508. Incorporation of this lipid into the PM model following the procedure used for ARC501-ARC507 leads to a lipid that exhibits a large overlap with the squalene molecules placed in the PM. In order to accommodate the squalene molecules, ARC508 was excluded from the PM.

After inclusion of the squalene residues in the hexagonal unit cell of the PM, a few bad contacts were found between the squalene residues and the PGP residues from neighboring trimer units. In order to remove these clashes, two dihedral angles in squalene were modified; the dihedral angle between atoms C15 and C14 was altered from a value of 49° (in SQU701 of structure S3) to 60°, and the dihedral angle between atoms C4 and C5 was changed from −54° to −19°.

*Arrangement of Glycolipids in the Inside-Trimer Compartment.* Three glycolipid molecules (GLC-AB, GLC-AC, and GLC−BC) are included in our unit cell model. These molecules correspond to the sulfated glycolipid molecules reported in S1 (see Table 1) and are located inside the trimer, on the extracellular side of the PM. GLC-AC faces bR monomers A and C, GLC-AB faces monomers A and B, while GLC−BC faces monomers B and C. The polar heads were taken from structure S1, and modified to obtain sulfated triglycoside lipids (S-TGA-1, or 3-$HSO_3$−Gal**p**$\beta$1-6Man**p**$\alpha$1-2Glc**p**$\alpha$-1-archeol). The polar head of GLC-BC, missing in S1, was constructed using the polar head of GLC-AC, and linked to the glycerol moiety of GLC-BC. The lipids GLC-AB, GLC-AC, and GLC-BC are shown in Figures 3 and 4.

An additional PGP lipid residue was placed in the intratrimer compartment, on the internal side of the membrane. Since there exists no glycolipid on the cytoplasmic part of the PM,[52] this internal intratrimer lipid was modeled as a PGP residue and labeled PGP-INTER. The lipid part of PGP-INTER was modeled using the conformation of dihydrophytol chains and the glycerol moiety of the GLC-AB residue.

*Hydration and Construction of the Hexagonal Unit Cell.* Water molecules were placed inside the unit cell bRs according to structure S3. For this purpose, S3 was superimposed on each monomer by minimizing the rms deviation between all $C_\alpha$ atoms per monomer; 69 water molecules were then placed into the three monomers at the positions suggested by the matched S3 structure. These water molecules are represented in Figure 5 as small orange spheres.

Additional water molecules were then added to the unit cell by filling the empty space external to proteins and lipids. For this purpose a cube of dimension 19 Å of equilibrated TIP3P water molecules was used to build a parallelepiped (water box) of dimension 75 Å (perpendicular to membrane plane) × 94 Å × 94 Å (parallel to membrane plane). The water box was superimposed on the unit cell, aligning centers and the orientation of respective Cartesian coordinate frames; the water box thus overlaid the three bR monomers, internal and external lipids as well as internal water molecules. The water molecules from the water box that have their oxygens closer than 2.6 Å to any heavy atom of the aforementioned components were deleted. No additional water molecules were added in the retinal binding site. The resulting water molecules exceeded the volume of the elementary cell. To repair this, a hexagonal prism of dimension 76.0 Å (perpendicular to membrane plane, extension *c)* × 60.8 Å × 60.8 Å (parallel to membrane plane, extensions *a* and *b*) was superimposed on the protein−lipid−water system in an obvious alignment. All water molecules of the water box external to the prism were deleted. The total number of water molecules per unit cell was 2804.

The hexagonal unit cell thus constructed was then replicated in three dimensions to model a macroscopic multilamellar PM system. The 60.8 Å dimension corresponds to the observed spacing in the two-dimensional crystalline PM.[13] The transmembrane dimension of $c = 76.0$ Å corresponds to an interlamellar spacing that is accessible to observation of multilamellar PMs. Experimentally observed *c* values depend on the hydration level and other conditions of sample preparation and vary from 55 Å (corresponding to about three interlamellar layers of water molecules),[38] to 80 Å (corresponding to about 10 interlamellar layers of water molecules).

*NVE and NpT Simulations of Periodic System.* Molecular

**TABLE 2: Results of Free Energy Perturbation Calculations on Water Molecules W1 to W5 placed in Monomeric bR (see Figure 1)[a]**

| water molecule | $\Delta A_{elec}$ (kcal/mol) | $\Delta A_{vdw}$ (kcal/mol) | $\Delta A_{total}$ (kcal/mol) | rms fluctuations (Å) | $k_{harm}$ (kcal/mol/Å$^2$) | probability of existence |
|---|---|---|---|---|---|---|
| W1 | 17.1 | −0.3 | 16.8 | 0.60 | 7 | 0.99 |
| W2 | 7.8 | 2.6 | 10.4 | 1.17 | 2 | 0.98 |
| W3 | 9.1 | 2.0 | 11.1 | 0.70 | 4 | 0.97 |
| W4 | 10.1 | −0.2 | 9.9 | 0.50 | 7 | 0.70 |
| W5 | 7.9 | 0.4 | 8.2 | 1.00 | 2 | 0.70 |

[a] The free energy of creation of a water molecule was calculated following ref 30. $\Delta A_{elec}$ and $\Delta A_{vdw}$, are the electrostatic and van der Waals contributions to the total free energy ($\Delta A_{total}$), respectively. The values of the rms fluctuations of water molecules around their average positions and the values of the harmonic constraints applied on the water molecules during the free energy perturbations calculations (see ref 30) are also given.

dynamics simulations described in this paper were carried out using the program NAMD, version 2.1,[53] with the exception of the free energy perturbation simulations that were carried out using the program CHARMM version 22.[47] Simulations assumed NVE ensembles that keep particle number *N,* volume *V*, and total energy *E* constant, corresponding to solutions of the Newtonian equations of motion, as well as NpT ensembles in which terms added to the Newtonian equations keep pressure and temperature constant. Pressure constancy is achieved through changing the size of the unit cell, i.e., through altering the extensions *a*, *b,* and *c* defined above.

NAMD2 permits full electrostatic, nonorthogonal periodic cell, and constant pressure simulations and runs effectively on workstation clusters. A dielectric constant $\epsilon = 1$ and an integration time step of 1 fs were chosen for this simulation. Short-range nonbonded interactions were smoothly switched to zero over the range 6−10 Å with interaction lists updated effectively every time step (i.e., no interactions were missed). Long-range electrostatic interactions were calculated using the smooth particle-mesh-Ewald method of Essmann et al.[54] The r-RESPA integrator[55] was employed so that nonbonded interactions could be calculated every other time step[56] and long-range electrostatic interactions could be calculated every fourth time step. After an initial energy minimization to remove bad initial contacts, the system was assigned initial velocities according to a Maxwell distribution and heated to 300 K in steps of 50 K by velocity reassignments every 0.5 ps over a 10 ps time period. The system was then allowed to equilibrate at 300 K by continued velocity reassignments every 10 ps over a 650 ps time period. The unit cell's dimensions *a, b,* and *c* were allowed to equilibrate at 1 atm over an additional 350 ps time period using a combination of Langevin dynamics for temperature control and a Langevin-thermostated Hové−Hoover constant pressure method.

Except for the retinal chromophore, the force field parameters were obtained from the CHARMm25b2 implementation of Quanta98. For the retinal moiety, parameters obtained from ab initio calculations on retinal analogues[57,58] were used as in refs 31 and 48.

## Results

Water molecules play an essential role in conducting protons and likely also in the mechanism of bR's proton pump. We have focused our present investigation on the distribution and dynamics of water in bR and in the PM. Below we describe first our findings for single bR and then for the entire PM.

**Simulation of Monomeric bR.** The questions which molecular modeling seeks to answer are (1) where is water located and (2) how does it alter its location during the pump cycle. We address these questions here for a bR monomer.

*Placement of Internal Water Molecules.* Figure 1 presents the location of stable water molecules in the equilibrated (300 K) bR monomer structure[31] and Table 2 lists the characteristics as determined from free energy perturbation calculations. Three water molecules (W1, W2, W3) are predicted to have a high probability (>0.9) of existence. These correspond indeed to well-resolved water molecules in the crystal structures reported in ref 16 and in ref 20. Water molecule W2, not given in the PDB entry 1AP9, but described in ref 16, was included in our calculations. This water molecule, although of high thermodynamic stability, exhibits larger rms fluctuations (1.2 Å) than other stable water molecules (e.g., 0.7 Å) and may thus show a poor electron density due to its thermal fluctuation, possibly explaining the controversy about its existence mentioned further above.

Water molecules W4 and W5 (cf. Figure 1 and Table 2), according to our calculations, have a lower thermodynamic stability. These water molecules correspond to water molecules reported in ref 16 that are not well resolved. Water molecule W4 forms a hydrogen bond with the hydrogen of C15 in retinal and was suggested to play a role in the photocycle.[30] A water molecule corresponding to W4 was previously found, using the structure determined by Grigorieff et al.,[13] to be very stable, with a probability of ∼1.[30] The difference in the calculated probabilities for W4 highlights the importance of the new crystal structure for water placement near retinal.

Water molecules W4 and W5 have not been included in the PM model, although the free energy calculations cannot rule out their existence.

*Water Rearrangement during the Photocycle.* Our simulations suggest that water rearrangement can take place when retinal changes its isomeric state in the course of the photocycle, in agreement with the recent structures of the K, L, and M intermediates.[21−23,25] Starting with a monomeric bR model as described above,[31] water rearrangement in the retinal binding site was investigated for *all-trans* and for 13-*cis* conformations of retinal using classical MD simulations on a nanosecond time scale. The photoisomerization was carried out by means of a modified torsional potential as described in ref 28. The time scale of the present simulation implies that the resulting structure corresponds to an early intermediate, as discussed in ref 21, rather than the L or M intermediates described in refs 22, 23, and 25.

Since only a monomeric bR was explicitly described in this calculation, the overall influence of the PM environment on a monomer's structure was modeled as follows: A harmonic constraint of 2 kcal/mol/Å$^2$ was applied on bR backbone atoms that were further than 18 Å away from the Schiff base nitrogen. These harmonic constraints were used in previous MD simulations of monomeric bR[30,31,39,48] to maintain the shape of the protein. In another set of simulations, no harmonic constraint

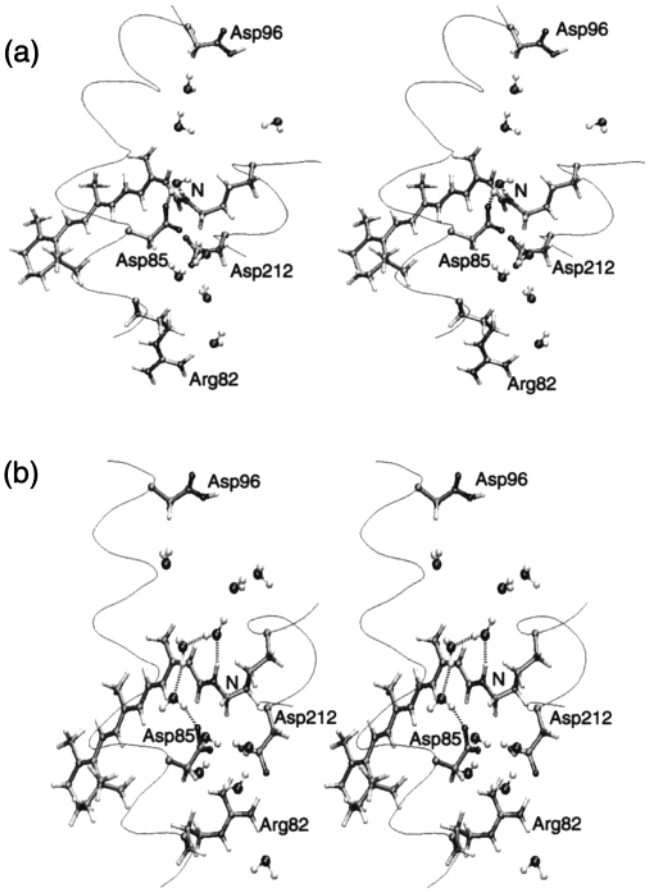


**Figure 6.** Water rearrangements after photoisomerization. Only those water molecules whose probability of occupation has been calculated and/or the water molecules that undergo rearrangement during the MD simulations are shown. Case (a): Water molecule W4 moved from the cytoplasmic half of the retinal binding site to bridge the Schiff base and Asp85. Arg82 is oriented "down". Case (b): Two water molecules moved from the extracellular half of the retinal binding pocket to bridge the Schiff base and Asp85. Arg 82 is oriented "up".

was applied and all atoms were allowed to move unconstrained, as in refs 28, 29, and 59.

Water movement was found to depend on two factors, the presence of harmonic constraints on bR backbone atoms and the isomerization state of retinal. No significant water rearrangement was found on a nanosecond time scale for bR with *all-trans* retinal, regardless of the presence or absence of harmonic constraints on the backbone atoms. No water rearrangement was observed during the simulations of bR with 13-*cis* retinal with harmonic constraints on the backbone. However, a significant rearrangement of water molecules was found in simulations on bR with 13-*cis* retinal as long as no harmonic constraints were applied. The resulting rearrangement, shown in Figure 6, involved the movement of a water molecule to a position perpendicular to the retinal plane. This water molecule had a different origin in different simulations carried out. In one case, the water molecule originated from the cytoplasmic channel, i.e., involved water W4 (see Figure 1), and in another case originated from the extracellular channel. Direct experimental evidence about the rearrangement of water molecules during the photocycle of bR has been provided in recent crystal structures of bR intermediates.[21,22]

In the present simulations, the hydrogen bond network between Asp85, Asp212, the retinal's Schiff base, and a water molecule is disrupted after *all-trans* to 13-*cis* isomerization of

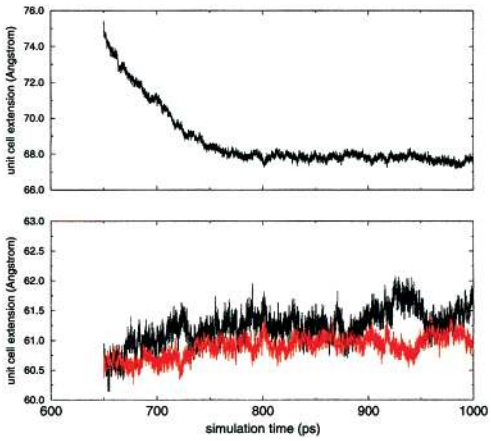


**Figure 7.** Variation of unit cell extensions during the constant pressure molecular dynamics simulation, i.e., during the last 350 ps of the 1 ns simulation. Top: variation of extension *c* (perpendicular to the membrane plane). Bottom: variations of the in-plane extensions *a* (black) and *b* (red).

the chromophore. A change in the hydrogen bond network in the vicinity of the Schiff base group is also evident from the recent structure for the K intermediate reported in ref 21. According to the electron density differences between the ground state and the K intermediate in this paper, a water molecule (W402), situated between the Schiff base and Asp85 in the ground state, is dislocated after isomerization. This water molecule is actually not resolved in the PDB file, but the reported difference maps[21] clearly indicate its displacement after isomerization.

In both cases of our simulations a hydrogen bond was established between the Schiff base proton, the displaced water molecule, and the side chain of Asp85. Significant conformational changes were also observed for the side chain of Arg82. In the case of a water molecule moving from the extracellular channel to the Schiff base region, Arg82 changed its orientation from pointing toward the extracellular side to pointing toward retinal. A downward movement of Arg82 has been reported in the recent structures of M intermediates,[22,25] and not in the structure of K.[21] The opposite direction of the Arg82 movement in the present simulations is probably due to an initial placement of water molecules in the extracellular channel that forces Arg82 to be downward in the ground state, as in ref 28. The results confirm that, when the hydration pattern is modified upon photoisomerization, Arg82 has enough flexibility to change its conformation according to water rearrangement.

These results suggest that under certain conditions water movement establishes a hydrogen bond network between the Schiff base and Arg82. These conditions are (a) photoisomerization of retinal, (b) protein flexibility (allowed in our model by the absence of harmonic constraints), and (c) side chain rearrangement.

The study of the isomerization of retinal and the subsequent events in bR requires a very careful examination. The nature of the applied potential, the starting configuration of the binding pocket, and the presence of any constraints in the simulation can significantly influence the conclusions. The harmonic constraints applied to regulate water movement in the present study are artificial. Clearly, a model of bR that includes its native PM environment is required for a cogent description of its pump cycle dynamics. Furthermore, we believe that application of improved potentials, such as QM/MM calculations, is necessary for a proper description of such events. The results of this section, however, provide theoretical evidence for the rear-

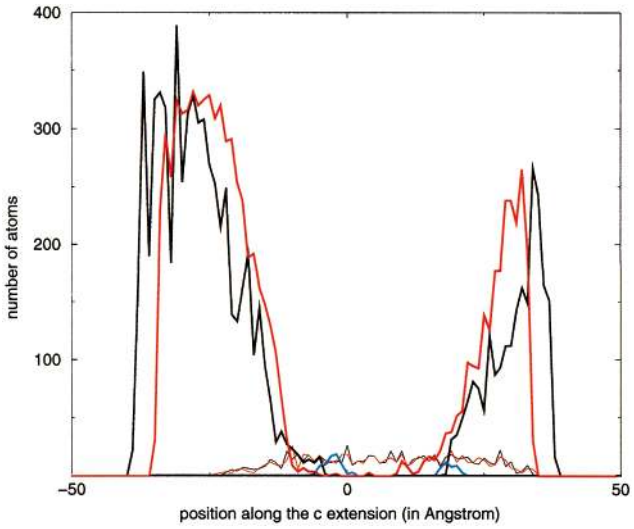


**Figure 8.** Atomic distributions of water and protein side groups along the *c* extension in the unit cell. Black: From PM structure before MD simulation. Red: From PM structure after 1 ns of MD simulation. Thin lines: distribution of $C_\alpha$ atoms in bR monomers. Thick lines: distribution of external water molecules' oxygen atoms. Thick blue lines: distribution of atoms of residues Asp96 and Arg82. The origin of the position corresponds to the $C_\alpha$, positions of Tyr56 in monomer B and Phe208 in monomer A.

rangement of water molecules during the photocycle, which is supported by experimental results.

**Equilibration of the PM.** After the PM model had been constructed as outlined in Methods, molecular dynamics simulations provided the system an opportunity to relax into a stable state and to redistribute, in particular, its water molecules. The relaxation observed will be described now.

*Constant-Pressure Simulation.* An MD simulation was performed on the complete PM model for 1 ns. NVE conditions were applied for the first 650 ps and NpT conditions with a pressure of 1 atm for the remaining 350 ps. Figure 7 shows the variation of the unit cell's dimensions during the NpT phase. One can discern that the *c* extension of the unit cell (perpendicular to the membrane plane) exhibits a significant decrease within about 100 ps from its original value of 75.4 Å to a value below 68.0 Å, after which the *c*-value fluctuated around an equilibrium value of 67.8 Å. The reduction of the *c* extension is due to a redistribution of water molecules placed externally at a safe distance from the protein and lipid components of the PM. We will show below that some water molecules enter interprotein space of the PM, reducing thereby the unit cell volume since the number N of all atoms is kept constant in our simulations.

During the NpT phase, also the *a* and *b* extensions of the unit cell were free to alter. Figure 7 shows that the initial values for *a* and *b* of 60.5 Å experience only small increases to 61.6 and 61.8 Å, respectively. Variations of *a* and *b* appear to be anti-correlated. The fluctuations of *a* and *b* around their equilibrium values are much smaller than the fluctuations of *c*. The equilibrium values of *a* and *b* are consistent with observations reported for different crystal structures with values ranging from 60.63 Å in ref 20 (S3) to 62.45 Å in ref 13 (S4).

*Behavior of External Water Molecules.* Figure 8 shows the distribution of the protein's $C_\alpha$ atoms along the *c* dimension of the unit cell, both for the starting structure and after 1 ns of simulation. The distributions are essentially identical, indicating that the protein is not compressed or expanded during the NpT phase of the simulation.

The distribution of external water molecules, both for the initial structure and after 1 ns of MD simulation, is shown in Figure 8. In the initial structure, the density of the external water molecules is very low in the region of the unit cell where protein atoms are present, and no external water molecules penetrate the protein deeper than regions corresponding to Arg82 on the extracellular side, and Asp96 on the cytoplasmic side. The distribution of external water molecules at the end of the simulation reveals the cause for the reduction of the *c* extension of the unit cell. As shown in Figure 9, water molecules penetrate the membrane into interprotein space, in particular into a region surrounded by helices A and G, and by extratrimer cytoplasmic lipid molecules PGP5 and PGP6 (and their images from neighboring trimers). On the time scale of the present simulation, no external water molecules move to the retinal binding site. However, the MD simulations on a monomeric bR model described above suggest that water molecules could possibly move from a level below Arg82 to the retinal binding site depending on the dynamics of Arg82, and depending on the isomerization state of retinal. Residues Asp96 and Arg82 appear to be acting as gates that define the intra- and extra-membrane regions of the PM and control the penetration of external water molecules in the protein during the pump cycle.

*Behavior of Internal Water Molecules.* The internal water molecules placed according to structure S3[20] exhibit during the ns simulation significantly different mobilities, depending on their initial location, as shown in Figure 10. The six water molecules located in the proton channel of the protein, between residues Asp96 and Arg82, i.e., water molecules labeled 401, 402, 406, 407, 502, and 501 in S3, remain in the channel during the simulation. Two water molecules that are located between Arg82 and the extracellular side of the PM (404 and 405 in S3) remain in the vicinity of Arg82. However, more distal water molecules of the extracellular part of the proton channel were found to diffuse into the extramembrane environment. In keeping with the stochastic nature of diffusion, the displacements of these water molecules differed between the three bR monomers.

## Discussion

With the availability of crystallographic structures at below 2 Å resolution, even of intermediates, research of bR has entered an exciting era that promises that the mechanism of proton pumping of bR will be discovered along with an explanation of bR's ability to switch off pumping at high transmembrane potentials. Research on bR has seen much less participation of theoretical researchers than other areas of biophysics, e.g., the areas of photosynthetic proteins or protein folding. With the available structures providing a solid foundation, the field should attract theoretical biologist who can contribute greatly to the understanding of the fundamental energy conversion process in bR. The present study demonstrates the opportunities that lie ahead.

Our calculations and the results presented above show what theoretical investigations can achieve today in the bR field. Molecular modeling tools can integrate crystallographic structures into an atom level model of the PM that can guide theoretical and experimental efforts. Nanosecond time scale molecular dynamics simulations of the intact structure of the PM model are technically feasible for full electrostatics and under NVE and NpT conditions. The calculations have become possible through a new generation of software, NAMD2,[53] that the authors' group has developed over the past decade and that it shares freely with other investigators. The simulations of the

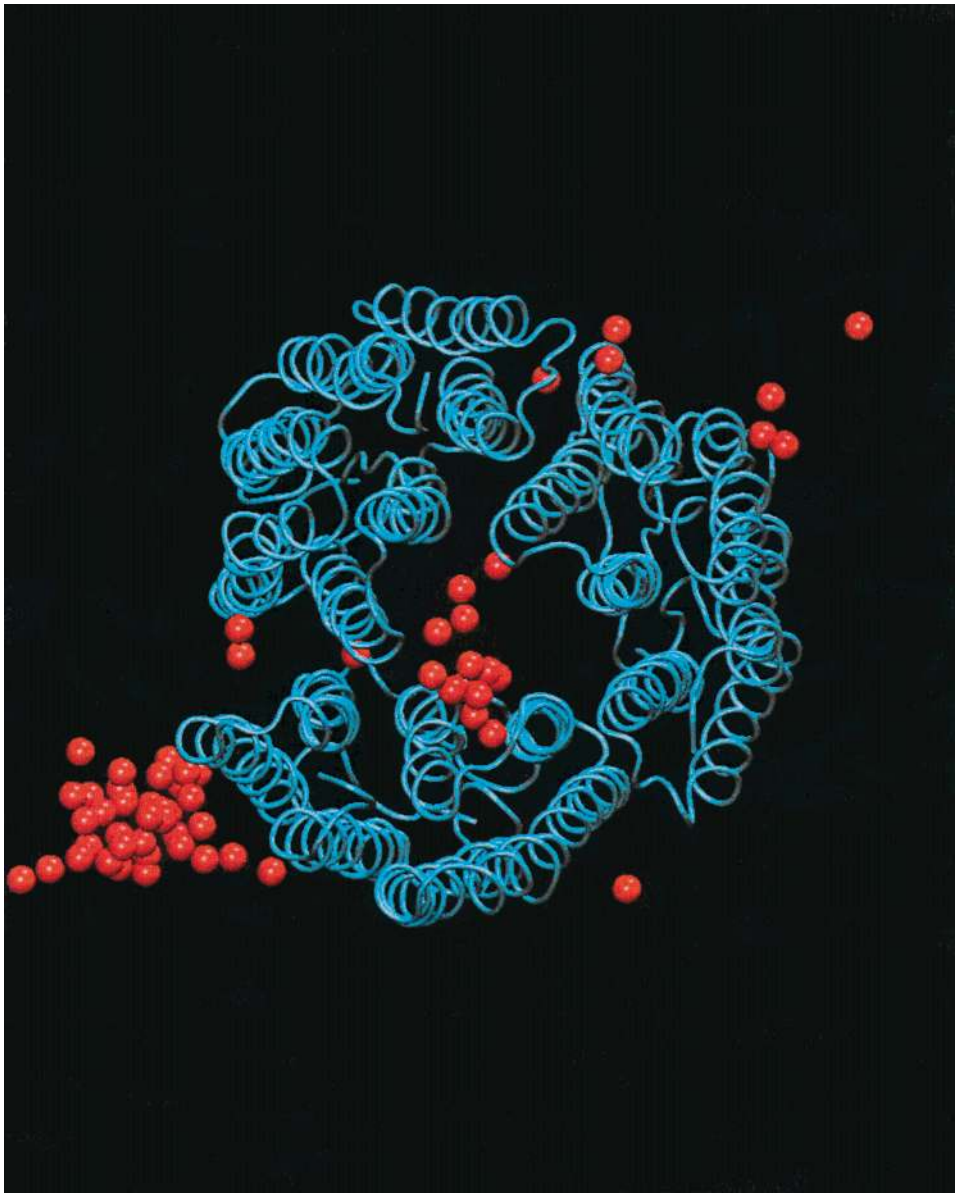

**Figure 9.** Top view (from cytoplasmic side) of the external water molecules that penetrated the membrane during the MD simulation. The bR monomers are shown in tube representation in blue; water molecules are presented as orange spheres.

PM described above provide valuable information of the distribution of all water molecules around bR, linking the retinal binding site and a few internal water molecules seamlessly with bulk water. Future simulations will be based on the PM model provided, possibly further improved, e.g., by using free energy perturbation calculations to complement crystallographic data for water molecules placement in bR. An example of the potential of such simulations to explain bR's pump mechanism is our study of the response of water molecules to conformational transitions in bR, presented above, that can reveal the switch mechanism needed for bR's pump action. Such transitions in the position and conformation of water molecules may be involved in the switch step of bR's pump action.

Progress not described here has been made in calculating ground and excited-state potential surfaces of retinal as reported in ref 60. These calculations revealed a simple picture for the key steps of retinal isomerizations: (1) a motion after light excitation from the Franck−Condon region to the nearest or most accessible minimum on the excited-state potential surface, e.g., located near the transition point for the *all-trans* → 13-*cis* transition; (2) a crossing through a nearby conical intersection governed by the torsional coordinate as well as a bond stretching coordinate to the ground-state surface; and (3) completion of the isomerization path to the 13-*cis* equilibrium state.

Despite the considerable progress in theoretical work on bR and the PM demonstrated in this paper, the main challenges lie still ahead. These challenges should attract theoretical researchers noting that on the one hand, PM is a fascinating bioenergetic device that converts light energy into a membrane potential using the simplest molecular realization of such process, and that on the other hand all components of this system are known in principle at atomic level detail, leaving no room for error due to speculation. The following tasks need to be accomplished to meet the challenge to eventually describe the function of the PM on theoretical grounds, thereby documenting true understanding of the mechanism: water potentials need to be improved; polarizabilities of protein components need to be accounted for; quantum chemistry calculations of retinal electronic states should be carried out simultaneously with simulations of the photoprocess, providing on the fly forces stemming from retinal's internal degrees of freedom; simulations should identify the nature of the early K intermediate; the time scale

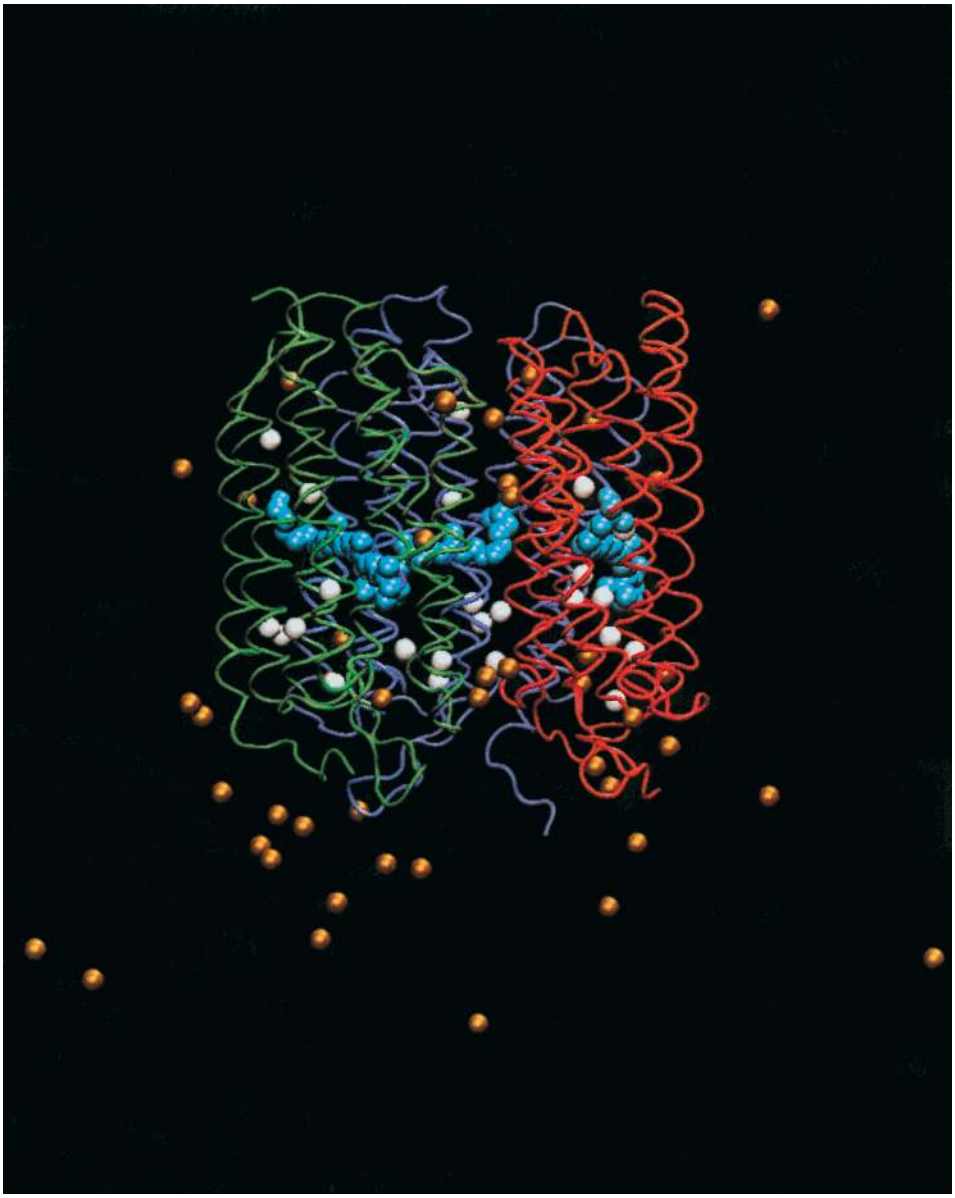

**Figure 10.** Location of crystallographic water molecules after 1 ns of MD. The external water molecules are not replicated periodically to simplify the view. In white: water molecules numbered 401, 402, 404, 405, 406, 407, 502, and 501 in crystal structure S3 that were found to stay in the retinal binding site or close to Arg82 during the MD simulation. In orange: crystallographic water molecules (from S3) that exchange with external water placed in constructing the PM model (see text). The bR monomers' backbones are displayed in red, blue, and green. Retinal moieties are shown in CPK representation.

of simulations should be extended to microseconds to reach the L intermediate and further extended to milliseconds to cover the complete pump cycle; electrostatics of bR should be faithfully described in the PM context; p*K* shifts of the retinal Schiff base and key side groups that arise during the pump cycle should be calculated; accurate methods for water placement should be developed and proton conduction be suitably described.

The progresses already made and the challenges outlined should convince computational biologists that studies of the PM can be intellectually rewarding and fruitful.

The structure of the PM presented in this paper will be available on request.

**Acknowledgment.** The authors would like to thank E. Pebay-Peyroula, H. Luecke, and L.O. Essen for making their structures available to us, B. Roux, J. C. Smith, and M. Nina for discussions on the free energy perturbations calculations, as well as M. Ben-Nun and T. J. Martínez for a collaboration on the quantum chemistry and quantum dynamics of bR. The authors acknowledge the Roy J. Carver Charitable Trust, the National Institute of Health (PHS 5 P41 RR05969-04), and the National Science Foundation (BIR-9318159; MCB-9982629).

## References and Notes

(1) Birge, R.; Cooper, T. M. *Biophys. J.* **1983**, *42,* 61.

(2) Logunov, S.; El-Sayed, M.; Song, L. *J. Phys. Chem.* **1996**, *100,* 2391.

(3) Ebrey, T. Light energy transduction in bacteriorhodopsin. In *Thermodynamics of Membranes, Receptors and Channels;* Jacobson, M., Ed.; CRC Press: New York, 1993.

(4) Lanyi, J. K. *FEBS Lett.* **1999**, *464*, 103.

(5) Schulten, K.; Humphrey, W.; Logunov, I.; Sheves, M.; Xu, D. *Isr. J. Chem.* **1995**, *35*, 447.

(6) Song, L.; El-Sayed, M. A.; Lanyi, J. K. *Science* **1993**, *261,* 891.

(7) Song, L.; El-sayed, M. A.; Lanyi, J. K. *J. Phys. Chem.* **1996**, *100,* 10479.
(8) Logunov, S.; El-Sayed, M.; Lanyi, J. *Biophys. J.* **1996**, *70,* 2875.
(9) Logunov, S. L.; Song, L.; El-Sayed, M. A. *J. Phys. Chem.* **1996**, *100,* 18586.
(10) Birge, R. R. *Annu. Rev. Phys. Chem.* **1990**, *41*, 683.
(11) Birge, R. R.; Gillepsie, N. B.; Kusnetow, A.; E. W. I. a.; Lawrence, A. F.; Singh, D.; Song, Q. W.; Schmidt, E.; Stuart, J. A.; Seetharaman, S.; Wise, K. J. *J. Phys. Chem.* **1999**, *103,* 10746.
(12) Henderson, R.; Baldwin, J. M.; Ceska, T. A.; Zemlin, F.; Beckmann, E.; Downing, K. H. *J. Mol. Biol.* **1990**, *213*, 899.
(13) Grigorieff, N.; Ceska, T.; Downing, K.; Baldwin, J.; Henderson, R. *J. Mol. Biol.* **1996**, *259,* 393.
(14) Kimura, Y.; Vassylyev, D. G.; Miyazawa, E.; Kidera, A.; Matsushima, M.; Mitsuoka, K.; Murata, K.; Hirai, T.; Fujiyoshi, Y. *Nature* **1997**, *389*, 206.
(15) Mitsuoka, K.; Hirai, T.; Murata, K.; Miyazawa, A.; Kidera, A.; Kimura, Y.; Fujiyoshi, Y. *J. Mol. Biol.* **1999**, *286,* 861.
(16) Pebay-Peyroula, E.; Rummel, G.; Rosenbusch, J. P.; Landau, E. M. *Science* **1997**, *227,* 1676.
(17) Lücke, H.; Richter, H. T.; Lanyi, J. K. *Science* **1998**, *280,* 1934.
(18) Essen, L.; Siegert, R.; Lehmann, W.; Oesterhelt, D. *Proc. Natl. Acad. Sci. U.S.A.* **1998**, *95,* 11673.
(19) Belrhali, H.; Nollert, P.; Royant, A.; Menzel, C.; Rosenbusch, J. P.; Landau, E. M.; Pebay-Peyroula, E. *Structure* **1999**, *7*, 909.
(20) Lücke, H.; Schobert, B.; Richter, H. T.; Cartailler, J. P.; Lanyi, J. K. *J. Mol. Biol.* **1999**, *291*, 899.
(21) Edman, K.; Nollert, P.; Royant, A.; Belrhali, H.; Pebay-Peyroula, E.; Hajdu, J.; Neutze, R.; Landau, E. M. *Nature* **1999**, *401,* 822.
(22) Luecke, H.; Schobert, B.; Richter, H. T.; Cartailler, J. P.; Lanyi, J. K. *Science* **1999**, *286*, 255.
(23) Royant, A.; Edman, K.; Ursby, T.; Pebay-Peyroula, E.; Landau, E. M. *Nature* **2000**, *406*, 645.
(24) Subramaniam, S.; Henderson, R. *Nature* **2000**, *406*, 653.
(25) Sass, H. J.; Büldt, G.; Gessenlich, R.; Hehn, D.; Neff, D.; Schlesinger, R.; Brendsen, J.; Ormos, P. *Nature* **2000**, *406,* 649.
(26) Zhou, F.; Windemuth, A.; Schulten, K. *Biochemistry* **1993**, *32,* 2291.
(27) Humphrey, W.; Logunov, I.; Schulten, K.; Sheves, M. *Biochemistry* **1994**, *33*, 3668.
(28) Humphrey, W.; Xu, D.; Sheves, M.; Schulten, K. *J. Phys. Chem.* **1995**, *99*, 14549.
(29) Xu, D.; Sheves, M.; Schulten, K. *Biophys. J.* **1995**, *69,* 2745.
(30) Roux, B.; Nina, M.; Pomes, R.; Smith, J. C. *Biophys. J.* **1996**, *71*, 670.
(31) Tajkhorshid, E.; Baudry, J.; Schulten, K.; Suhai, S. *Biophys. J.* **2000**, *78,* 683.
(32) Kandori, H.; Yamazaki, Y.; Sasaki, J.; Needleman, R.; Lanyi, J. K.; Maeda, A. *J. Am. Chem. Soc.* **1995**, *117*, 2118.
(33) Yamazaki, Y.; Hatanaka, M.; Kandori, H.; Sasaki, J.; Karstents, W. J.; Raofs, J.; Lugtenburg, J.; Bizarnok, M.; Herzfeld, J.; Needleman, R.; Lanyi, J.; Maeda, A. *Biochemistry* **1996**, *35*, 6308.
(34) Hatanaka, M.; Sasalo, J.; Kandori, H.; Ebrey, T.; Needleman, R.; Lanyi, J.; Maeda, A. *Biochemistry* **1996**, *35,* 6308.
(35) Hatanaka, M.; Kandori, H.; Maeda, A. *Biophys. J.* **1997**, *73,* 1001.
(36) Garavelli, M.; Vreven, T.; Celani, P.; Bernardi, F.; Robb, M. A.; Olivucci, M. *J. Am. Chem. Soc.* **1998**, *120,* 1285.
(37) Joshi, M. K.; Dracheva, S.; Mukhopadhyay, A. K.; Bose, S.; Hendler, R. W. *Biochemistry* **1998**, *37,* 14463.
(38) Zaccaï, G. *J. Mol. Biol.* **1987**, *194,* 569.
(39) Ferrand, M.; Zaccaï, G.; Nina, M.; Smith, J. C.; Etchesbest, C.; Roux, B. *FEBS Lett.* **1993**, *327,* 256.
(40) Fitter, J.; Lechner, R.; Dencher, N. *Biophys. J.* **1997**, *73,* 2126.
(41) Lehnert, U.; Réat, V.; Weik, M.; Zaccaï, G.; Pfister, C. *Biophys. J.* **1998**, *75,* 1945.
(42) Réat, V.; Patzelt, H.; Ferrand, M.; Pfister, C.; Oesterhelt, D.; Zaccai, G. *Proc. Natl. Acad. Sci. U.S.A.* **1998**, *95,* 4970.
(43) Edholm, O.; Berger, O.; Jehnig, F. *J. Mol. Biol.* **1995**, *250,* 95.
(44) Hofacker, I.; Schulten, K. *Proteins: Struct., Funct., Genet.* **1998**, *30,* 100.
(45) Yoshikawa, S.; Shinzawa-Itoh, K.; Nakashima, R.; Yaono, R.; Yamashita, E.; Inoue, N.; Yao, M.; Fei, M. J.; Libeu, C. P.; Mizushima, T.; Yamaguchi, H.; Tomizaki, T.; Tsukihara, T. *Science* **1998**, *280,* 1723.
(46) Rothschild, K. J.; Braiman, M. S.; He, Y. W. *J. Biol. Chem.* **1990**, *265,* 16985.
(47) Brooks, B. R.; Bruccoleri, R. E.; Olafson, B. D.; States, D. J.; Swaminathan, S.; Karplus, M. *J. Comput. Chem.* **1983**, *4*, 187.
(48) Baudry, J.; Crouzy, S.; Roux, B.; Smith, J. C. *Biophys. J.* **1999**, *76*, 1909.
(49) Crouzy, S.; Baudry, J.; Smith, J. C.; Roux, B. *J. Comput. Chem.* **1999**, *20,* 1644.
(50) Hartmann, R.; Sickinger, H. D.; Oesterhelt, D. *FEBS Lett.* **1977**, *82*, 1.
(51) Barnett, S. M.; Dracheva, S.; Hendler, R. W.; Levin, I. W. *Biochemistry* **1996**, *35,* 4558.
(52) Henderson, R.; Jubb, J. S.; Whytock, S. *J. Mol. Biol.* **1978**, *123,* 259.
(53) Kalé, L.; Skeel, R.; Bhandarkar, M.; Brunner, R.; Gursoy, A.; Krawetz, N.; Phillips, J.; Shinozaki, A.; Varadarajan, K.; Schulten, K. *J. Comput. Phys.* **1999**, *151*, 283.
(54) Essmann, U.; Perera, L.; Berkowitz, M. L.; Darden, T.; Lee, H.; Pedersen, L. G. *J. Chem. Phys.* **1995**, *103,* 8577.
(55) Tuckerman, M.; Berne, B. J.; Martyna, G. J. *J. Chem. Phys.* **1992,** *97*, 1990.
(56) Watanabe, M.; Karplus, M. *J. Phys. Chem.* **1995**, *99,* 5680.
(57) Nina, M.; Roux, B.; Smith, J. C. *Biophys. J.* **1995**, *68,* 25.
(58) Baudry, J.; Crouzy, S.; Roux, B.; Smith, J. C. *J. Chem. Inf. Comput. Sci.* **1996**, *37*, 1018.
(59) Ben-Nun, M.; Molnar, F.; Lu, H.; Phillips, J. C.; Martinez, T. J.; Schulten, K. *Faraday Discuss.* **1998**, No. 110, 447.
(60) Molnar, F.; Ben-Nun, M.; Martinez, T. J.; Schulten, K. *J. Mol. Struct. (THEOCHEM)* **2000**, *506,* 169.
(61) Humphrey, W. F.; Dalke, A.; Schulten, K. *J. Mol. Graphics* **1996**, *14*, 33.